Journal of Materials Chemistry A

Accepted Manuscript

ROYAL SOCIETY OF CHEMISTRY

www.rsc.org/materialsA

Journal of Materials Chemistry A RSCPublishing

PAPER

Impact of Alkoxy Chain Length on Carbazole-based, Visible Light-driven, Dye Sensitized Photocatalytic Hydrogen Production

Cite this: DOI: 10.1039/x0xx00000x

Received 00th January 2012,
Accepted 00th January 2012

DOI: 10.1039/x0xx00000x

www.rsc.org/

Motonori Watanabe[*a], Hidehisa Hagiwara[a,b], Yudai Ogata[b], Aleksandar Staykov[a], Sean R. Bishop[a], Nicola H. Perry[a], Yuan Jay Chang,[c] Shintaro Ida[a,b], Keiji Tanaka[a,b], Tatsumi Ishihara[*a,b]

Alkoxyphenyl-substituted carbazole-based metal-free organic dyes were synthesized and effectively used for dye-sensitized, visible-light-driven, photocatalytic hydrogen production. Photocatalytic hydrogen production was investigated using a TiO_2/dye/Pt structure with triethanolamine as the sacrificial reagent. The dye-loaded TiO_2 photocatalyst exhibited a high yield of hydrogen production when the length of the alkoxy chain was long enough to sufficiently improve the hydrophobicity at the interface between the dye-loaded TiO_2 and the water medium. In the alkoxyphenyl-substituted carbazole dyes, the dye with the longest alkoxy chain (**C22**) exhibited the best hydrogen production performance, but it had a yield only slightly better than that of the dye with the second longest chain length (**C16**). The dye **C22** displayed a turnover number (TON) of 3094 after 24 h of visible light irradiation (>420 nm). However, the compound with no hydrophobic substituent (**C1**), exhibited the lowest hydrogen production performance with a TON of 1497. Thus, a 207% increase in the hydrogen production yield was observed when hydrophobic substituents were present. Analysis of time-resolved absorption spectra, impedance spectra and incident photon conversion efficiency spectra revealed that the alkoxy chain has a hydrophobic effect at the interface between the dye-loaded TiO_2 and the water. Specifically, the hydrophobicity of the dye improved the charge-recombination lifetime for electron injection from the dye into the TiO_2 surface in the water for hydrogen production.

Introduction

Production of hydrogen is key for establishing clean energy systems because it can be used as a clean energy source in hydrogen fuel cells.[1,2] Hydrogen production using solar light-based catalysts is an ideal generation method because it is a simple and clean reaction: i) only a photocatalyst, sunlight and water are required; ii) the reaction occurs under mild conditions (even room temperature) and iii) water is split into hydrogen without producing carbon dioxide as a byproduct. Although this method has many environmental advantages, many challenges must be overcome before photocatalytic water splitting can be practically implemented. Most current photocatalysts do not exhibit good water splitting activity when exposed to visible light and require ultraviolet (UV) light because of their large energy band gaps. A photocatalyst that can utilize visible light would be more effective because UV light accounts for only 7% of sunlight, while visible light accounts for 47%, and the remaining energy falls in the near-infrared (IR) region of the electromagnetic spectrum. Some semiconductors with reduced band gaps obtained by modifying their valence state of the metal cations or through doping have exhibited visible-light-driven photocatalytic water-splitting activity. [3,4] For example, the semiconductor Ta_3N_5 exhibited water-splitting activity when exposed to light of wavelengths up to 600 nm. [5]

An alternative approach involves the use of dye-sensitized photocatalysts. This method may cover the visible range, because the molecular structures of organic dyes can be readily modified. [6,7] In a dye-sensitized hydrogen production in water with electron donor system, the organic dye absorbs the visible-light component of sunlight and becomes excited, leading to injection of an electron into the conduction band of the semiconductor, which then enables hydrogen production from water-containing electron donor (with a co-catalyst for increasing the hydrogen production yield). Dyes with suitable absorption and HOMO-LUMO energies can be selected by modifying their electronic structures to match the conduction band/valence band level of the photocatalyst. A variety of dyes for hydrogen production from water decomposition have been developed, including a Pt/TiO_2/dye system with a ruthenium complex, [8] porphyrin, [9] coumarin, [10] cyanine, [11] and xanthene[12] as the dye. To improve the hydrogen production yield in dye-sensitized, water-splitting cell systems, an understanding of the mechanism of the water decomposition reaction is needed. To improve the hydrogen production efficiency, a reduction in hole-electron recombination between the dye and TiO_2, and electron trapping after injection of the electrons from dye at the excited state, using e.g.,water or a sacrificial reagent, is an important issue. Kim et al. reported that a tin-porphyrin dye showed radical species lasting long enough (< 30 μs) on TiO_2 for hydrogen production.[24] We have

studied the spacer effect of benzo[b] phenothiazine-containing dyads[13] on hydrogen production. [14] The spacer is considered to decrease the charge recombination rate between the electron donor and the semiconductor, leading to enhancement of the hydrogen production amount. Han et al. reported that a hydrophilic substituent on the dye led to a decrease of the charge recombination rate because of interactions between the hydrophilic group and the water medium that in turn led to relaxation at the excited state. [15] This long-lived charge recombination improves the hydrogen production. Lee et al. also reported that the introduction of an alkyl chain in phenothiazine improved the hydrogen production performance. Although the reason for the effect of the alkyl chain on the yield of hydrogen production was unclear, they proposed that the orientations of the dyes on the TiO_2 were changed and resulted in acceleration of smooth electron injection, reduction of the decomposition reaction rate during the excited state of the dye and electron injection into the semiconductor and/or regeneration of the dye using sacrificial reagents. [16] Other factors affecting the yield of hydrogen production include the temperature, solvent medium and the stability of the photocatalyst. In the present study, we investigated the visible-light-driven water decomposition hydrogen production of carbazole-based, metal-free organic dyes with alkoxy substituents on the carbazole moiety with varying chain lengths. The carbazole moiety is one of the good electron donor moieties in the donor-spacer-acceptor systems such as in dye-sensitized solar cells.[40] In particular, the hydrophobic effect of the alkxoy chains on the hydrogen production yield was evaluated (Fig.1). A 207% increase in the hydrogen production yield was observed for the dye with the longest alkoxy chain compared to that for the dye with the shortest alkoxy substituent.

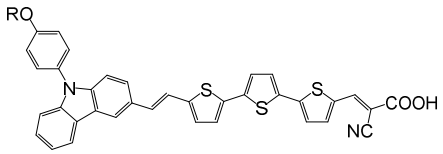

C1: R = -CH_3 **C16: R = -$C_{16}H_{33}$**
C6: R = -C_6H_{13} **C22: R = -$C_{22}H_{45}$**

Fig. 1 Series of synthesized dyes **C1-C22**.

Results and Discussion

Synthesis

Dyes **C1**, **C6**, **C16** and **C22** were synthesized from 9H-carbazole (**1**) (Scheme 1). The N-position of the carbazole was substituted with 4-alkoxyphenyl groups via coupling with 1-bromo-4-(alkoxy)benzene derivatives in the presence of K_2CO_3 using CuI/L-proline as the catalyst. The desired alkoxybenzene carbazoles (**2a–d**) were obtained in 9%–51% yield. The carbazoles (**2a–d**) were then subjected to Vilsmeier-Haack reaction conditions to afford the corresponding aldehydes (**3a–d**) in 41%–57%. Subsequently, the aldehydes (**3a–d**) were reduced using $NaBH_4$ and then reacted with triphenylphosphine hydrobromide to give the Wittig salts (**4a–d**) in 67%–98% over the two steps. The Wittig salts (**4a–d**) were then reacted with terthiophene-dicarboxyaldehyde to afford aldehydes (**5a–d**) in 64%–78%. Finally, these aldehydes were converted via Knoevenagel condensation to donor (carbazole)-spacer (terthiophene)-acceptor (cyanoacrylic acid) moieties (**C1–C22**) in 34%–67%. Further synthetic details are explained in the ESI†.

Physical properties

Absorption and fluorescence spectra

The absorption spectra of the dyes were obtained for 3.0×10^{-5} M THF solutions. The lowest energy bands of the dyes were observed at
457–460 nm for **C6**, **C16** and **C22**, while that of the dye **C1** was slightly blue-shifted (Fig 2 left). These lowest energy bands were assigned to the characteristic charge-transfer (CT) bands between the donor carbazole and acceptor cyanoacrylic acid groups in the dyes. The fluorescence spectra of the dyes in THF solutions included peaks at 549–553 nm for **C6**, **C16** and **C22**, while the peak for **C1** was once again slightly blue-shifted (542 nm). Based on the 0-0 offset bands, it was determined that all of the dyes had similar energy band gaps (2.39–2.40 eV) and HOMO-LUMO energies.

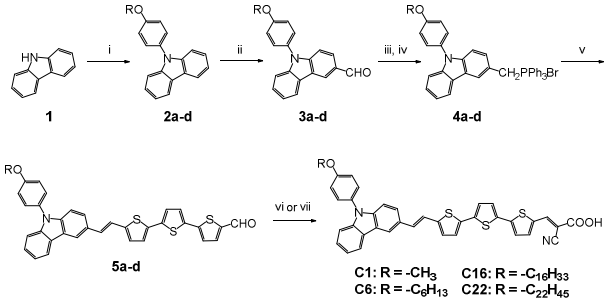

Scheme 1. Synthetic scheme of dyads **C1-C22**.
i) K_2CO_3, DMSO, L-proline, CuI, 1-bromo-4-alkoxybenzene. 9-51%; ii) $POCl_3$, DMF. 41-57%; iii) $NaBH_4$, THF-MeOH, then iv) triphenylphosphane hydrobromide, toluene. 67-98% in 2 steps; v) [2,2':5',2"-terthiophene]-5,5"-dicarbaldehyde, K_2CO_3, 18-crown-6-ether, DMF. 64-78% vi) cyanoacetic acid, ammonium acetate, AcOH.; vii) cyanoacetic acid, ammonium acetate, THF-AcOH. 34-67%.

Cyclic voltammetry

To examine the HOMO and LUMO energies of dyes **C1–C22**, cyclic voltammetry experiments were performed (Fig. 2 right). One reversible electron oxidation at $E_{1/2}^{ox}(I)$ = 1.17 V (vs. NHE.) was observed for **C1**, while the $E_{1/2}^{ox}(I)$ = values for **C6**, **C16** and **C22** were all found to be 1.16 V (vs. NHE). However, no irreversible reduction potentials were observed to −1.0 V in the THF potential window (V vs NHE). The LUMO energies of dyes **C1–C22** were estimated to be −1.23 to −1.24 V (V vs NHE) from the 0-0 offset bands that were estimated from overlap position between absorption and fluorescence spectra. In addition, only a very small difference in the oxidation potentials was found for **C1** and the other three dyes (**C6**, **C16** and **C22**), indicating that the electron donating ability of the alkoxy chain to the dye backbone can be neglected, particularly for the dyes with long alkoxy chains, i.e. **C6**, **C16** and **C22**.

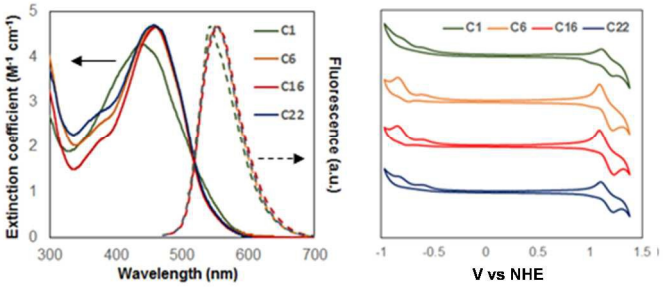

Figure2. Absorption spectra of dyes **C1–C22** in THF (3.0×10^{-4} M) (left), Cyclic voltammograms of **C1–C22** in 0.1 M Bu_4NPF_6-containing THF solutions. The scan rate was 100 mV/s. (right)

Table 1. Experimental and calculated parameters of all dyes.

Comp.	λ_{max} nm[a] (ε/$M^{-1}cm^{-1}$)	FL (nm)	0-0 band (nm) / eV	HOMO/LUMO[b] (V vs NHE)[c]	Comp abs (*f*)[d]	Comp HOMO/LUMO (eV)[d]
C1	438 (42700)	542	517 / 2.40	1.17/-1.24	499.88 (2.0766)	-5.79/-2.08
C6	459 (46700)	549	516 / 2.40	1.16/-1.24	501.64 (2.0864)	-5.77/-2.08
C16	460 (46700)	553	518 / 2.39	1.16/-1.23	501.80 (2.0967)	-5.77/-2.08
C22	457 (47000)	550	517 / 2.40	1.16//-1.24	501.70 (2.0937)	-5.77/-2.08

a : Measured in THF, b : LUMO calculated by HOMO + E_{0-0},
d : Obtained by TDDFT at the BhandLYP/6-31G(d) level
c : Calibrated according to Fc/Fc^{+} = - 0.63 V vs. NHE.

Theoretical computations for molecules

The absorption, fluorescence and CV spectra of all of the dyes indicated that they had similar photophysical and electrochemical properties. The optimized structures of **C1-C22** were obtained by B3LYP/6-31G(d) basis set. Time-dependent density functional theory (TD-DFT) calculations were performed for the HOMO and LUMO energies at the B3LYP[17] or BHandHLYP[17] or M06[26] functions with the 6-31G(d) basis set. All of the trends of HOMO-LUMO energies and gaps, and oscillator strength were the same as the experimental data trends. In these theoretical results, BHandHLYP showed much closer energy gaps with experimental (Table S1†), and results suggested that nearly all of the HOMOs and LUMOs were delocalized on the donor-terthiophene and terthiophene-cyanoacrylic acid moieties, respectively. However, no contribution to the HOMO-LUMO levels was found for the alkoxybenzene moieties. The lowest energy absorption bands for all of the dyes were attributed to the HOMO-LUMO levels, suggesting charge-transfer-type interactions. For the dye **C1,** the lowest energy band and HOMO-LUMO levels were estimated to be approximately 500 nm and −5.79/ −2.08 eV, respectively, while the values for the other three dyes were approximately 502 nm and −5.77/ −2.08 eV, respectively.

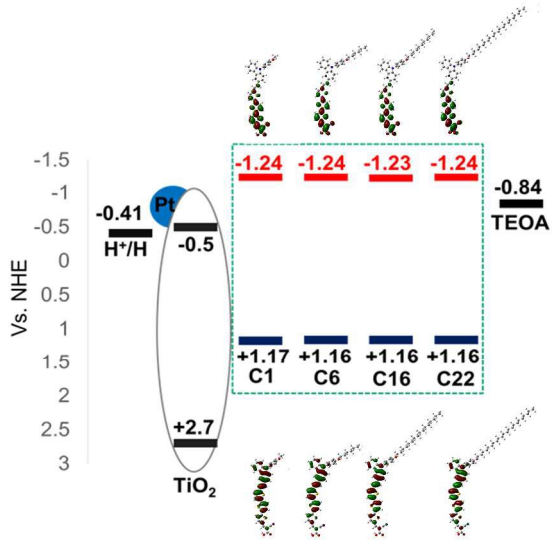

Figure3. Potential energy levels of dyes and generated molecular orbitals of HOMO and LUMO geometries from the optimized structure of **C1–C22** at the BHandHLYP/6-31G(d) level.

The trends in the calculated lowest energy bands, oscillator strengths and HOMO-LUMO energies agreed well with those observed experimentally. These results indicated that the alkoxy groups had little electron-donating or electron-accepting abilities, but the absorption structure and HOMO-LUMO gaps were not changed (Fig. 3). The physical and theoretical properties are summarized in Table 1.

Hydrogen production

Visible-light-driven (>420 nm, 300 W Xe lamp) hydrogen production was evaluated using a dye (**C1–C22**)/ TiO_2/ 1 wt% co-catalyst system in water (10% triethanolamine (TEA), pH = 7). All of the reactions were performed for 24 h. The hydrogen production performance with several co-catalysts, i.e. Pt, Au, RuO_2, NiO, and without a co-catalyst (w/o) was compared using dye **C16** (Figure S1† and Table S2†). We found that the order of hydrogen production was Pt (1405 μmol) > Au (142 μmol) > RuO_2 (66 μmol) > NiO (56 μmol) > w/o (9 μmol). The results suggested that the extraction of electrons from the dye could be promoted by the co-catalyst. The trends can be explained by the order of the work functions: Pt (5.65-5.32 eV)[27] > Au (5.10 eV)[27a] > RuO_2 (4.8 – 5.04 eV)[28] > NiO (3.8 – 5.0 eV)[29], and no help of electron promotion (w/o), because a larger work function can promote the electron acceptor properties.[30]

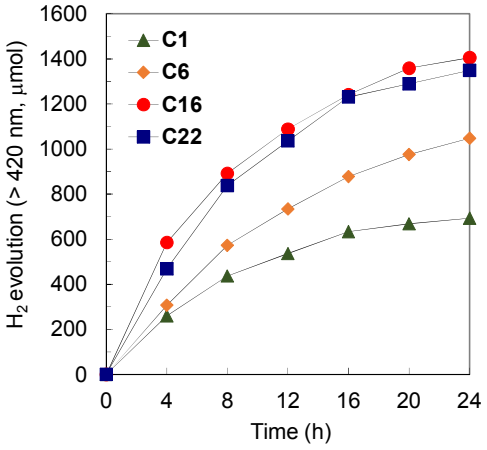

Figure4. Photocatalytic activities of dyes **C1-C22** in hydrogen production from water. Reaction conditions: 10 vol% aqueous TEA (10 mL), 33.0 mg dye/ TiO_2 /Pt catalyst, pH = 7.0.

Table 2. Photocatalytic performance[a], decay lifetimes, and impedance results (resistances) of all dyes on TiO_2

Comp.	Dye-loading (μmol /33 mg)	H_2 amount (μmol)[b] / TON[c]	τ_1 (ps)	τ_2 (ps)	τ_3 (ps)	R_1 (ohms)	R_2 (ohms)
C1	0.927	694 / 1497	1.07	8.52	89.2	11.9	205.2
C6	0.904	1048 / 2319	1.79	11.8	99.0	11.1	222.7
C16	0.959	1405 / 2930	1.42	16.7	127.0	11.5	293.4
C22	0.872	1349 / 3094	1.06	10.1	111.2	10.9	249.3

a: A 300 W Xe lamp was used and wavelengths below 420 nm were cut off using an optical fillter. b: H_2 produced after 24 h.
c : TON = (2 × amount of H_2 / dye loading amount after 24 h)/amount of dye.

The effects of dyes were further examined with a dye (**C1–C22**)/ TiO_2/ 1 wt% Pt system in water (10% triethanolamine (TEA), pH = 7). The highest hydrogen production yield was observed for **C16**, which exhibited an amount of the hydrogen production of 1405 μmol, and the hydrogen production yield was found to differ in the order **C16** (1405 μmol) > **C22** (1349 μmol) > **C6** (1048 μmol) > **C1** (694 μmol). After correcting for the number of dye molecules loaded on the photocatalyst, the turnover numbers were found to be 1497 for **C1**, 2319 for **C6**, 2390 for **C16** and 3094 for **C22** (Fig.4).
In dye sensitized photocatalytic hydrogen production, the extinction coefficient, absorption range of dye, and HOMO-LUMO energy levels of the dye are important properties to modify in order to improve the absorption of the light energy. The LUMO energy positions affect the driving force of electron injection from the exited dye to the CB of TiO_2. The absorption properties of the various dyes were quite slimmer. Furthermore, the LUMO energies of the dyes were similar, relative to the CB of TiO_2 (Fig 3). These results suggested that the effect of the electronic properties of the dyes does not account for the difference yields of hydrogen production. Lee et al. reported that alkyl chain substituents on phenothiazine dyes used in dye-sensitized water decomposition cells may improve the hydrogen production yield because of suppression of the rate of decomposition of the dye itself and/or its reaction with water or a change in the orientation of the dye on the TiO_2 surface.[16] As can be seen in Fig.4., all the hydrogen production decay profiles of the four dyes were quite similar, which suggested that the alkoxy chains did not influence the decomposition pathway. It is considered that hydrophilic substituents on the dyes would improve the charge recombination lifetime of the excited states, while hydrophobic groups would not be expected to have a strong influence in water.

Time-resolved absorption spectra
To elucidate the reason for the improvement in the TON with increasing chain length of the alkoxy substituent, time-resolved absorption spectra were recorded. The spectra were obtained using a dye-loaded TiO_2 film (approximately 8–10 nm thick on a quartz plate) that was dipped in pure water (pH = 7). It can be seen in Fig.5 that the solid-state absorption spectra for the dyes on TiO_2 were similar.
The time-resolved absorption spectra of **C22** on the TiO_2 film in water (pH=7) revealed that a rise of a broad peak (600 to 750 nm) maximized around 690 nm was observed on a time scale of 1 ps or even longer. It exhibited absorption above approximately 600 nm for the radical cation species, while a negative peak was observed below 600 nm induced by ground-state bleaching (Fig. 6a).[18] In addition, all the dyes were found to exhibit triple exponential decay functions, and the time decay constants for compounds **C1–C22** fell in similar ranges (Fig.6b), i.e. τ_1 = 1.07–1.79 ps, τ_2 = 8.52–16.7 ps and τ_3 = 89.2–127.0 ps. These decay lifetimes are in good agreement with those observed previously for oligo-thiophene-containing dye-loaded TiO_2 systems.[14] Han et al. have reported that the electron injection from dyes into TiO_2 sites occurs on a time scale of hundreds of femtoseconds. A long charge recombination time of greater than 5 ps would allow electron injection from the dye into the conduction band of TiO_2, while species remaining less than 5 ps of would indicate a charge recombination process between dye and TiO_2 at the surface and/or shallow traps on TiO_2.[15, 19]
In dye-sensitized solar cell systems, it has been reported that when the angle of orientation of the dye on the TiO_2 surface is large, the charge recombination lifetime and efficiency decrease dramatically because of through-space charge recombination between the dye and the TiO_2 surface.[20, 21]

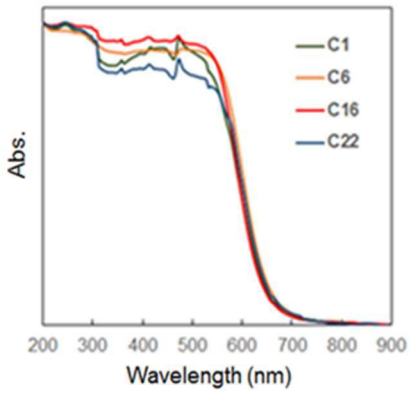

Figure 5. Solid state absorption spectra of dye-loaded **(C1-C22) TiO_2** film.

The lifetimes of the four dyes investigated in the present study were found to fall in the order of C16 (16.7 ps) > C6 (11.8 ps) ≧ C6 (10.1 ps) > C1 (8.52 ps) for τ_2, and the radical cation species survived in the order of C16 (127.0 ps) > C22 (111.2 ps) > C6 (99.0 ps) > C1 (89.2 ps) for τ_3. Han et al. reported that a hydrophilic substituent on the dye led to a dramatic decrease of the charge recombination rate by relaxation with water.[15] In our results, no change of the structure of signal positions in the time-resolved absorption spectra at the range of 0 to 150 ps was confirmed. This result suggested that the effect of the alkoxy chain length for relaxation with water solvent was small.

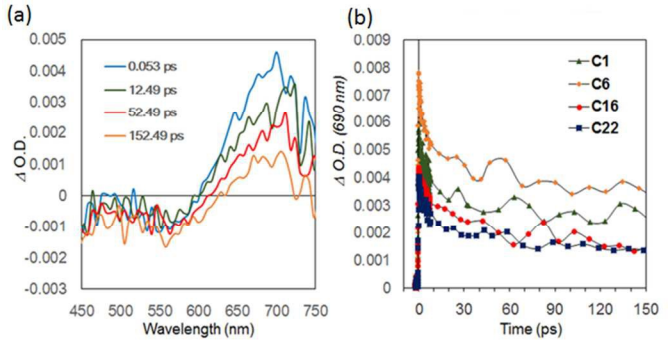

Figure 6. (a) Typical time-resolved absorption spectra of **C22-loaded TiO_2** film in water (pH = 7) condition, and (b) time decay profile of dye-loaded (**C1-C22) TiO_2** at 690 nm in the range of -10 to 150 ps.

The orientation of the dye on TiO_2 is controlled by the connecting mode of dye to TiO_2, and the perpendicular structure is favourable to reduce the charge recombination lifetime.[34, 35]

Dye-TiO_2 Surface Calculation Results

Calculations of the dye on the TiO_2 surface were performed using density functional theory with plane wave basis set implemented in the Vienna Ab-initio Software Program (VASP) with PBE functional.[31-33]

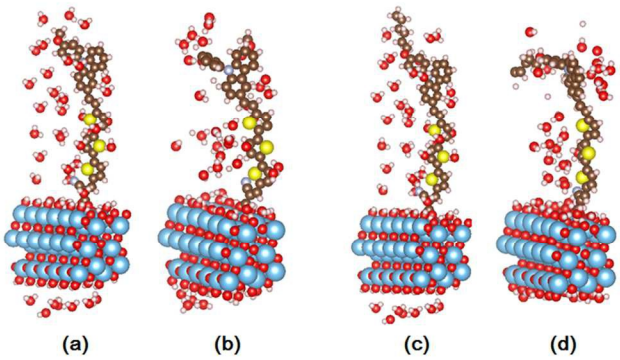

Figure 7. First principle molecular dynamics results of (a, b) **C1** and (c, d) **C6** on TiO_2 (101) surface with 50 water molecule. The snapshots at (a) 0 ps for **C1** on TiO_2, (b) after 1.8 ps, and (c) 0 ps for **C6** onTiO_2, (d) after 2.5 ps.

During the geometry optimization a 300 eV cut-off energy was employed with Monkhorst- Pack automatic 1 × 2 × 1 k-points sampling. The periodic cell has dimensions of 22.7 Å × 10.2 Å × 50 Å and contains 479 atoms for **C1** with TiO_2. The TiO_2 was modelled with three layers of the anatase surface with (101) Miller indices. All surface oxygen atoms were hydrogen terminated in order to avoid a surface induced dipole moment. During the optimization the coordinates of the middle layer were kept fixed while the coordinates of the top and bottom layers were fully relaxed. Due to the high cost of computation when a long-alkyl chain is attached, we examined the molecule **C1** for optimization. The organic dye was connected at the surface to Ti atoms through Ti-O bonds at bidentate geometry with 82.9° for **C1** on TiO_2 of dihedral angle between TiO_2 surface and cyanoacrylic acid moiety, suggested perpendicular to the surface. (Figure S2†)

To understand the dynamics of the organic dyes on the TiO_2 surface in water medium, first principles molecular dynamics (MD) simulations were performed for the organic dye attached to the anatase surface and 50 water molecules. The early stage structure of **C1** used the structure optimization gave. The early stage structure of **C6** used the one which changed the alkoxy group of the optimization structure of **C1** to a hexyloxy group. The simulations were performed with PBE theory implemented in the VASP program and 300 eV cut-off energy. The time step was 1.0 fs and the simulation time was 1.8 ps for **C1** on TiO_2. The dye **C6** extended calculation until 2.5 ps to check influence of a hexyloxy group. The simulation temperature was kept constant at 300 K. The snapshots are shown in Figure 7. Although during the MD simulation, the carbazole moiety on the molecule and its alkoxy chain were periodically rotating, the dye molecules were perpendicular to the surface and there were only insignificant deviations from the early stage geometry, suggested that the dye was keeping the standing position at 300 K with water molecules.

Impedance and Incident Photon to Current Conversion Efficiency (IPCE) spectra

To gain further insight into the influence of the alkoxy chain on improving the charge recombination and hydrogen production amount, electrochemical impedance spectra (EIS) of the dye-loaded TiO_2 films were obtained using a three electrode cell (working electrode/reference electrode/counter electrode) system.

The dye-loaded TiO_2 film coated on fluorine-doped tin oxide (FTO) glass was used as the working electrode, a Pt mesh was used as the counter electrode, and Ag/AgCl was used as the reference electrode. An aqueous Co^{2+}/Co^{3+} solution was used as the electrolyte. The small, high frequency semicircles in the range of 1–20 ohms seen in the inset of Fig.8 (left) have been attributed to the electrode/electrolyte impedance. On the other hand, major semicircular arcs related to charge recombination at the interface between the TiO_2 and dye/electrolyte were observed in the low frequency range (~20–300 ohms resistance).[22] The diameter of the largest semicircles decreased in the order **C16** (293.4 ohms) > **C22** (249.3 ohms) > **C6** (222.7 ohms) > **C1** (205.2 ohms). These results are in reasonable agreement with the results obtained for the yields of hydrogen production; it is possible that the water medium trapped the electrons when the hydrophobicity was decreased. Although the length of the alkoxy chain in **C22** was greater than that for the other dyes, its hydrogen production and charge recombination rates were lower and faster, respectively, than those for **C16**. However, the amount of dye in **C22** loaded onto the TiO_2 (0.872 μmol/33 mg TiO_2) was the lowest of all of the four dyes. These results, therefore, suggested that the packing structure for **C22** on the TiO_2 surface was not well defined because of the longer length of the alkoxy chain. They may also provide an indication of the orientation of **C22** on the TiO_2. If the electron trapping was suppressed at the interface of solvent and dye/TiO_2, because of the alkoxy chain, the overall efficiency of electron correction from the dye to the TiO_2 surface would be increased.[35, 36]

To determine the overall light to current efficiency, IPCE spectra were obtained for the dye-loaded TiO_2 films and are shown in Fig 8 (right) over the range from 350–750 nm. IPCE results combined the light-to-current efficiency from light harvesting, electron injection efficiency, and electron correction efficiency.[37] Although the IPCE cannot evaluate these components separately, over the entire range, the charge transfer efficiencies followed the order **C16** > **C22** > **C6** > **C1**, confirming that dye **C16** exhibited the highest photons-to-current efficiency. These results also indicated that the length of

the alkoxy chain is important and should be designed to achieve a good hydrophobic effect for dye-sensitized hydrogen production reactions from water.

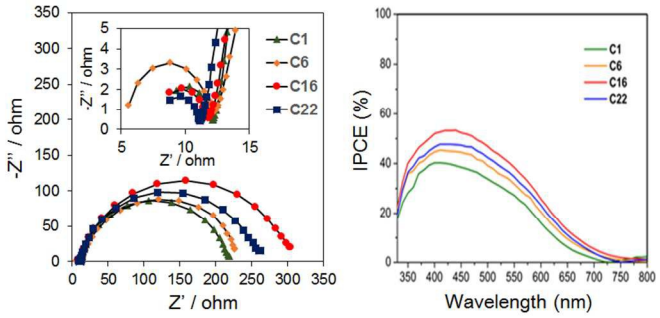

Figure 8. EIS Nyquist plot of dye-loaded TiO_2 at 0 V bias under illumination (left). IPCE plots of dye-loaded TiO_2 (right).

Conclusions

Novel donor–spacer–acceptor dyads with 4-alkoxybenzene substituents on the donor carbazole units were synthesized for investigation of the hydrophobic effect of the alkoxy chains in dye-sensitized hydrogen production reaction from water. Their properties were in good agreement with the values obtained using DFT calculations. While barely any changes in the HOMO-LUMO gaps and electron-donating abilities of dyads **C1–C22** were observed, the visible-light-driven photocatalytic hydrogen production of dye/ TiO_2/Pt catalysts at pH 7 in 10% aqueous TEA differed for the four dyes. The hydrogen production yield increased as the length of the alkoxy chain increased, and the highest hydrogen production yield (measured as the TON) was observed for **C22** (3094), while the lowest yield was found for **C1** (1497). Overall, a 207% increase in the hydrogen production yield was observed because of the incorporation of a hydrophobic substituent into the dyads. On the other hand, the hydrophobic substituents did not improve the stability of the catalysts, and the deactivation times for all the compounds were approximately 24 h. In addition, the time-resolved absorption spectra for all the dyes on TiO_2 exhibited triple-decay components, and the longest decay component behaved in a similar manner to that of the hydrogen production yield for the four dyes, suggesting that the charge recombination lifetime was affected by the different alkoxy chain lengths. EIS analyses indicated that the dye **C16** had the longest charge recombination lifetime between the TiO_2 and dye/electrolyte, while that of **C1** was the shortest. Finally, the IPCE spectra indicated the same trend as observed in the EIS plots, suggesting that the alkoxy chain enhanced electron injection from the dye into the TiO_2. Furthermore, the hydrogen production yield for dye **C22** with the longest alkoxy group was nearly saturated, as was that for **C16**, because the dye-packing structures on the TiO_2 in these two systems was not well defined because of the longer alkoxy chains. This reduced packing order on the TiO_2 enabled easy contact with the water at the water/TiO_2 interface. Therefore, we have demonstrated that hydrogen production via visible-light-driven dye-sensitized hydrogen production can be increased through the use of hydrophobic effects at the interface of the photocatalyst and the water medium.

Experimental Section

The ^1H and ^{13}C NMR were recorded on a BrukerAV600 (600 MHz). The ^1H and ^{13}C NMR chemical shifts were reported as d values (ppm) relative to external Me_4Si. The coupling constants (J) were given in hertz. MALDI mass spectra were recorded on a Bruker Auto flex. The sample was dissolved in dichloromethane first, then equal amounts of this sample solution (1.0 m L) and a dithranol in dichloromethane (DIT, 1.0 m L) were spotted onto the stainless steel sample plate for injection together. High resolution mass spectra were recorded on a JEOL LMS-HX-110 spectrometer. FAB MS spectra were recorded with 3-nitrobenzyl alcohol (NBA) as the matrix. Analytical thin layer chromatography (TLC) was performed on Silica gel 60 F 254 Merck. Column chromatography was performed on KANTO Si60N (neutral). Absorption spectra were recorded on a SIMAZU IR spectrophotometer. IR spectra were recorded on a SHIMAZU spectrometer. Redox potentials were carried out on a BAS-100B/W electrochemical analyser. CV measurements were performed using a cell equipped with glassy carbon as the working electrode, platinum wire as the counter electrode, and $Ag/AgNO_3$ as the reference electrode. All electrochemical measurements were performed under an Ar atmosphere at room temperature in THF solution (5×10^{-4} M) containing 0.10 M tetra-n-butylammoniumhexafluoro-phosphate (Bu_4NPF_6) as a supporting electrolyte at a scan rate of 100 mV s^{-1}. The ferrocene/ferrocenium (Fc/Fc+) couple was used as an internal standard. THF was distilled from sodium benzophenone ketyl. Toluene was distilled from CaH_2. Other solvents and reagents were of reagent quality, purchased commercially, and used without further purification.

Dye-Loading process into 1wt% Pt loaded TiO_2 anatase

The procedure of 1.0 wt% Pt-loaded TiO_2 was as follows in accordance with the literature.[23] The commercially available TiO_2 source (1.0 g, <25 nm, anatase) was added to MeOH (25 mL) and H_2PtCl_6 (0.25 mL, 8 wt%). The mixture was irradiated using a Xe lamp (300 W) for 25 min, leading to the production of TiO_2 – Pt nanoparticles. The TiO_2 – Pt nanoparticles were separated by centrifugation (3600 rpm, 20 min); the separated TiO_2 – Pt nanoparticles were filtered, washed with MeOH successively, and then dried under vacuum, resulting in the production of Pt-loaded TiO_2 nanoparticles.

1.0 wt% Pt-loaded TiO_2 (100 mg) was immersed in a MeOH solution containing 3×10^{-4}M dye sensitizers (10 mL) for 24 h in the dark. The solvent was removed by centrifuged (3600 rpm, 20 min) and filtration, rinsed with anhydrous MeOH. The powder of dye-loaded TiO_2 catalyst was dried under vacuum. It was used for hydrogen production reaction without further treatment.

Hydrogen Production Reaction

The photocatalytic hydrogen production experiment was performed with a conventional closed circulating system with a dead volume of approximately 500 mL. The dye/TiO_2 /Pt catalyst (33 mg) was suspended in 10 mL of 10 v/v% triethanolamine water (pH = 7.0, adjust with HCl aq.). A quartz reaction cell was irradiated using an external light source comprising a 300 W Xe lamp (Ushio Inc., Japan) with <420 nm cut off glass filter. During the H_2O photochemical reaction, the reaction mixture was mixed using a magnetic stirring bar. The amount of H_2 gas was measured with a TCD gas chromatograph (GC-8A, Shimadzu Corp., Japan), which was connected to a conventional volumetric circulating line with a vacuum pump.

Time transient absorption measurements
The titania-oxide pastes of Ti-Nanoxide T/SP that was purchased from Solaronix. The quartz plate (transmission > 90% in the visible) was used as substrate. A thin film of TiO_2 (8–10 mm) was coated on a quartz substrate. It was immersed in an anhydrous THF solution containing 3 x 10^{-4} M dye sensitizers for at least 24 h, then rinsed with anhydrous THF and dried. Time transient absorption spectra of dyes on thin-film or in solution were performed in an ambient atmosphere. The femtosecond transient absorption data were collected with a pump and probe transient absorption spectroscopy system (Ultrafast Systems, Helios). The pump light (400 nm) was used from an amplified Ti-sapphire laser system (Spectra-Physics, Solstice-100F, < 100 fsec, 5 kHz). The UV/Vis range (350-750 nm) was detected with a linear CCD array (Ocean Optics, S2000). The triple exponential decay model was used for fitting. (eq. 1)

$$|\Delta OD/\Delta OD_0| = A_1 exp\left[-\frac{t}{\tau_1}\right] + A_2 exp\left[-\frac{t}{\tau_2}\right] + A_3 exp\left[-\frac{t}{\tau_3}\right] \quad (1)$$

Fabrication of Dye-loaded TiO_2 coated FTO glass
Dye-loaded TiO_2 coated FTO glass was used as working electrode, which has 3 x 2 cm dimension of FTO glass with *8 Ω/sq* as surface resistivity, and has 7 x 7 mm dimension (8 um thick) of TiO_2 layer. The TiO_2 layer (Ti-Nanoxide T/SP, SOLARONIX) was screen-printed on FTO glass. The TiO_2-coated FTO glass was pre-dried 1 h at 100 ^oC, followed by heated 80 min at 500 ^oC in air condition. It was immersed in an anhydrous THF solution containing 3 x 10^{-4} M dye sensitizers for at least 24 h, then rinsed with anhydrous THF and dried, to give Dye-loaded TiO_2 coated FTO glass.

Electrochemical Impedance Spectra (EIS) measurements
The experimental configuration for the EIS measurements consisted of a working electrode/ reference electrode / counter electrode system. Dye-loaded TiO_2 coated FTO glass was used as working electrode. Pt mesh was used as counter electrode. The reference electrode used was Ag/AgCl. An aqueous solution of 0.16 M $Co[(bpy)_3](NO_3)_2$, 0.032 M $Co[(bpy)_3](NO_3)_2$, and 0.08 M KCl served as the electrolyte. EIS measurements were performed using a Novocontrol Alpha analyzer with a ZG4 interface at 0V bias voltage at 59 $\pm$ 2 ^oC, with a frequency range from under room-light illumination. The equivalent circuit is Gerischer element[22] and analysis was performed by Z-view software.

IPCE measurement
For the measurement of IPCE was carried out by the structure of Dye-loaded TiO_2 coated FTO/electrolyte / Pt system. The electrolyte was used by LiI (0.05 M), I_2 (0.05 M), and TBP (0.5 M) in MeCN at 25^oC.

Theoretical Computation

Geometry optimization of the dyes were accomplished by Gaussian G09 (Rev. C. 01) program[38], and dye chemisorbed on the anatase surface was performed using the DFT implemented in the VASP program with PBE functional. Throughout this study, we have used the graphical visualization package VESTA to analyze and visualize the computed DFT results.[39]

Acknowledgements
This work was supported by a Grant-in-Aid for Science Research (YB 26810107) from the Ministry of Education, Culture, Sports, Science and Technology (MEXT), Japan, and was performed under the Cooperative Research Program of "Network Joint Research Centre for Materials and Devices (IMCE, Kyushu University)". MW, AS, SRB, and NHP acknowledge support from I^2CNER, funded by the World Premier International Research Centre Initiative (WPI), Ministry of Education, Culture, Sports, Science and Technology of Japan (MEXT), Japan.

Notes and references
[a] *International Institute for Carbon-Neutral Energy Research (I2CNER),Kyushu University, 744 Motooka, Nishi-ku, Fukuoka 819-0395, Japan*
[b] *Department of Applied Chemistry, Kyushu University, 744 Motooka, Nishi-ku, Fukuoka, 819-0395, Japan*
[c] *Department of Chemistry, Tung Hai University, Taichung 407, Taiwan*

† Electronic Supplementary Information (ESI) available: [Synthetic detail of dyes (C1-C22), and ^1H and ^{13}C NMR spectra, hydrogen production test with different co-catalyst.]. See DOI: 10.1039/b000000x/

1. A. J. Bard and M. A. Fox, *Acc. Chem. Res.,* **1995,** *28,* 141.
2. C. Song, *Catal. Today,* **2006**, *115*, 2.
3. M. Ni, M. K. H. Leung, D. Y. C. Leung and K. Sumathy, *Renewable Sustainable Energy Rev.,* **2007,** *11,* 401.
4. A. Kudo and Y. Miseki, *Chem. Soc. Rev.,* **2009,** *38,* 253.
5. M. Hihashi, K. Domen, and R. Abe, *Energy Environ. Sci.,* **2011,** *4,* 4138.
6. W. J. Youngblood, S.-Y. A. Lee, K. Maeda and T. M. Mallouk, *Acc. Chem. Res.,* **2009,** *42,* 1966
7. J. R. Swierk and T. E. Mallouk, *Chem. Soc. Rev.,* **2013,** *42,* 2357.
8. (a) E. Borgarello, J. Kiwi, E. Perlizzetti, M. Visca and M. Grätzel, *Nature,* **1981**, *289,* 158; (b) T. Kajiwara, K. Hashimoto, T. Kawai and T. Sakata, *J. Phys. Chem.,* **1982,** *88,* 4516; (c) Y. I. Kim, S. J. Atherton, E. S. Brigham and T. E. Mallouk, *J. Phys. Chem.,* **1993**, *97,* 11802; (d) K. Hirano, E. Suzuki, A. Ishikawa, T. Moroi, H. Shiroishi and M. Kaneko, *J. Photochem. Photobiol., A,* **2000,** *136*, 157; (e) K. Maeda, M. Eguchi, W. J. Youngblood and T. E. Mallouk, *Chem. Mater.,* **2008,** *20,* 6770; (f) X. Zhang, U. Veikko, J. Mao, P. Cai and T. Peng, *Chem.–Eur. J.,* **2012,** *18,* 12103; (g) H. Luo, W. Song, P. G. Hoertz, K. Hanson, R. Ghosh, S. Rangan, M. K. Brennaman, J. J. Concepcion, R. A. Binsteas, R. A. Bartynski, R. Lopez and T. J. Mayer, *Chem. Mater.,* **2013,** *25,* 122.
9. W. Kim, T. Tachikawa, T. Majima, C. Li, H-J. Kim, and W. Choi, *Energy Environ. Sci.,* **2010,** *3,* 1789.
10. R. Abe, K. Sayama and H. Arakawa, *J. Photochem. Photobiol., A,* **2004,** *166,* 115.
11. R. Abe, K. Shinmei, K. Hara and B. Ohtani, *Chem. Commun.,* 2009, 3577.
12. (a) T. Shimizu, T. Iyoda and Y. Koide, *J. Am. Chem. Soc.,* **1985,** *107,* 35; (b) X. Zhang, Z. Jin, Y. Ki, S. Li and G. Lu, *J. Phys. Chem. C,* **2009,** *113,* 2630; (c) P. Chowdhury, H. Gomaa and A. K. Ray, *Int. J. Hydrogen Energy,* **2011,** *36,* 13442.
13. M. Watanabe and T. Ishihara, *Acta Cryst.,* **2014,** *E70,* o1026.
14. M. Watanabe, H. Hagiwara, A. Iribe, Y. Ogata, K. Shiomi, A. Staykov, S. Ida, K. Tanaka and T. Ishihara, *J. Mater. Chem. A,* **2014,** *2,* 12952.
15. W.-S. Han, K.-R. Wee, H.-Y. Kim, C. Pac, Y. Nabetani, D. Yamamoto, T. Shimada, H. Inoue, H. Choi, K. Cho and S. O. Kang, *Chem.–Eur. J.,* **2012,** *18,* 15368.
16. J. Lee, J. Kwak, K. C. Ko, J. H. Park, J. H. Ko, N. Park, E. Kim, D. H. Ryu, T. K. Ahn, Y. J. Lee and S. U. Son, *Chem. Commun.,* **2012,** *48,* 11431.
17. A. D. Becke, *J. Chem. Phys.,* **1993,** *98,* 1372.
18. R. Bereram, R. V. Grondelle and J. T. M. Kennis, *Photosynth. Res.,* **2009,** 101, 105.
19. A. furube, T. Asahi, H. Masuhara, H. Yamashita and M. Anpo, *J. Phys. Chem. B* **1999,** *103,* 3120.
20. A. S. Hart, C. B. KC., H. B. Gobeze, L. R. Sequeria, and F. D'Souza, *ACS Appl. Mater. Interfaces,* **2013,** *5,* 5314.

21. (a) H. Imahori, S. Kang, H. Hayashi, M. Haruta, H. Kurata, S. Isoda, S. E. Canton, Y. Infahsaeng, A. Kathiravan, T. Pascher, P. Chábera, A. P. Yartsev and V. Sundström, *J. Phys. Chem. A,* **2011,** *115,* 3679.; (b) S. Ye, A. Kathiravan, H. Hayashi, Y. Tong, Y. Infahsaeng, P. Chabera, T. Pascher, A. P. Yartsev, S. Isoda, H. Imahori and V. Sundström, *J. Phys. Chem. C,* **2013,** *117,* 6066.
22. Q. Wang, J-E. Moser, and M. Grätel, *J. Phys. Chem. B,* **2005,** *109,* 14945.
23. D. P. Hagberg, T. Edvinsson, T. Marinado, G. Boschloo, A. Hagfeldt and L. Sun, *Chem. Commun.,* **2006,** 2245.
24. W. Kim, T. Tachikawa, T. Majima, C. Li, H-J. Kim and W. Choi, *Energy Environ. Sci.* , **2010,** *3* , 1789.
25. A. D. Becke, *J. Chem. Phys.*, **1993,** *98,* 5648.
26. Y. Zhao and D. G. Truhlar. *Theor. Chem. Acc.,* **2008,** *120,* 215.
27. a) L. Pintilie, I. Vrejoiu, D. Hesse and M. Alexe, *J. Appl. Phys.* 2008, *104,* 114101. b) L. V. Whitney, *Phys. Rev.* **1936,** *50,* 1154.
28. a) M. Tomkiewicz, Y. S. Huang and F. H. Pollak, *J. Electrochem. Soc.* **1983,** *130*, 1514.; b) H. C. Zhong, G. Heuss and V. Misra, *IEEE Electron Device Lett.,* **2000,** *21,* 593; c) S. Han, S. K. Kim, C. S. Hwang, *ECS Transaction,* **2010,** *33,* 111.
29. a) I. M. Chan, T-Y. Hsu and F. C. Hong, *Appl. Phys. Lett.,* **2002** 81, 1899.; b) K. Nakaoka, J. Ueyama and K. Ogura, *J. Electroanal. Chem.*, **2004,** *571,* 93.; c) J. M. McKay and V. E. Henrich, *Phys. Rev. B,* **1985,** *32,* 6764.
30. Y. Mizukoshi, Y. Makise, T. Shuto, J. Hu, A. Tominaga, S. Shironita and S. Tanabe, Ultrason Sonochem, **2007,** *14,* 387.
31. G. Kresse and J. Hafner, *Phys. Rev. B* **1993,** *47,* 558.
32. G. Kresse and J. Furthmueller, *Phys. Rev. B* **1996,** *54,* 11169.
33. G. Kresse and J. Furthmueller, *Comput. Mater. Sci.* **1996,** *6,* 15.
34. a) T. Higashino and H. Imahori, Dalton trans., 2015, 44, 448.; b) A. S. Hart, B. K. C. Chandra, H. B. Gobeze, L. R. Sequeira and F. D' Souza, *ACS Appl. Mater. Interfaces,* **2013**, *5,* 5314.; c) H. Imahori, S. Kang, H. Hayashi, M. Haruta, H. Kurata, S. Isoda, S. E. Canton, Y. Infahsaeng, A. Kathiravan, T. Pascher, P. Chábera, A. P. Yartsev and V. Sundström, *J. Phys. Chem. A,* **2011,** *115,* 3679.; d) S. Ye, A. Kathiravan, H. Hayashi, Y. Tong, Y. Infahsaeng, P. Chabera, T. Pascher, A. P. Yartsev, S. Isoda, H. Imahori and V. Sundström, *J. Phys. Chem. C,* **2013,** *117,* 6066.
35. J. E. Kroeze, N. Hirata, S. Koops, Md. K. Nazeeruddin, L. Schmidt-Mende, M. Grätzel and J. R. Durrant, *J. Am. Chem. Soc.,* **2006,** *128,* 16376.
36. .L. Schmidt-Mende, J. E. Kroeze, J. R. Durrant, Md. K. Nazeeruddin and M. Grätzel, *Nano Lett.,* **2005,** *7,* 1315.
37. M. Grätzel, *Acc. Chem. Res.,* **2009,** *42,* 1788.
38. M. J. Frisch, G. W. Trucks, H. B. Schlegel, G. E. Scuseria, M. A. Robb, J. R. Cheeseman, G. Scalmani, V. Barone, B. Mennucci, G. A. Petersson, H. Nakatsuji, M. Caricato, X. Li, H. P. Hratchian, A. F. Izmaylov, J. Bloino, G. Zheng, J. L. Sonnenberg, M. Hada, M. Ehara, K. Toyota, R. Fukuda, J. Hasegawa, M. Ishida, T. Nakajima, Y. Honda, O. Kitao, H. Nakai, T. Vreven, J. A. Montgomery, Jr., J. E. Peralta, F. Ogliaro, M. Bearpark, J. J. Heyd, E. Brothers, K. N. Kudin, V. N. Staroverov, T. Keith, R. Kobayashi, J. Normand, K. Raghavachari, A. Rendell, J. C. Burant, S. S. Iyengar, J. Tomasi, M. Cossi, N. Rega, J. M. Millam, M. Klene, J. E. Knox, J. B. Cross, V. Bakken, C. Adamo, J. Jaramillo, R. Gomperts, R. E. Stratmann, O. Yazyev, A. J. Austin, R. Cammi, C. Pomelli, J. W. Ochterski, R. L. Martin, K. Morokuma, V. G. Zakrzewski, G. A. Voth, P. Salvador, J. J. Dannenberg, S. Dapprich, A. D. Daniels, O. Farkas, J. B. Foresman, J. V. Ortiz, J. Cioslowski, and D. J. Fox, Gaussian, Inc., Wallingford CT, 2010.
39. K. Momma and F. Izumi, *J. Appl. Crystallogr.* **2011,** *44,* 1272.
40. N. Koumura and K. Hara, *Heterocycles,* **2013,** *83,* 275.

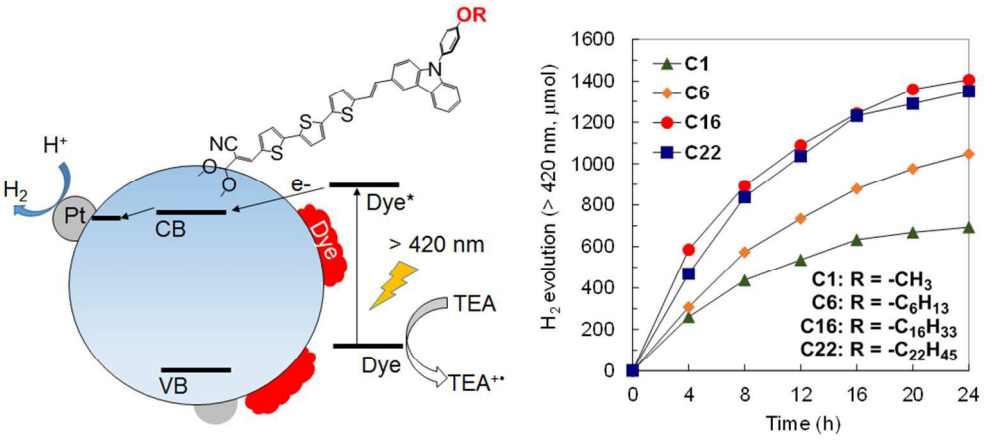

185x82mm (144 x 144 DPI)